GL-TR-89-0345
INSTRUMENTATION PAPERS, NO. 339

Laboratory Study of Ion-Neutral Collisions at Suprathermal Energies

JAMES A. GARDNER
RAINER A. DRESSLER
RICHARD H. SALTER
EDMOND MURAD

28 December 1989

SPACE PHYSICS DIVISION PROJECT 2303
GEOPHYSICS LABORATORY
HANSCOM AFB, MA 01731-5000

"This technical report has been reviewed and is approved for publication"

CHARLES P. PIKE, Chief
Spacecraft Interactions Branch

FOR THE COMMANDER

CHARLES P. PIKE, Acting Director
Space Physics Division

This report has been reviewed by the ESD Public Affairs Office (PA) and is releasable to the National Technical Information Service (NTIS)

Qualified requestors may obtain additional copies from the Defense Technical Information Center. All others should apply to the National Technical Information Service.

If your address has changed, or if you wish to be removed from the mailing list, or if the addressee is no longer employed by your organization, please notify GL/IMA, Hanscom AFB, MA, 01731. This will assist us in maintaining a current mailing list.

Do not return copies of this report unless contractual obligations or notices on a specific document requires that it be returned.

UNCLASSIFIED

SECURITY CLASSIFICATION OF THIS PAGE

REPORT DOCUMENTATION PAGE

Form Approved OMB No. 0704-0188

1a. REPORT SECURITY CLASSIFICATION UNCLASSIFIED	1b. RESTRICTIVE MARKINGS
2a. SECURITY CLASSIFICATION AUTHORITY	3. DISTRIBUTION / AVAILABILITY OF REPORT Approved for public release; Distribution unlimited
2b. DECLASSIFICATION / DOWNGRADING SCHEDULE	
4. PERFORMING ORGANIZATION REPORT NUMBER(S) GL-TR-89-0345 IP, NO. 339	5. MONITORING ORGANIZATION REPORT NUMBER(S)
6a. NAME OF PERFORMING ORGANIZATION Geophysics Laboratory 6b. OFFICE SYMBOL (If applicable) PHK	7a. NAME OF MONITORING ORGANIZATION
6c. ADDRESS (City, State, and ZIP Code) Hanscom AFB Massachusetts 01731-5000	7b. ADDRESS (City, State, and ZIP Code)
8a. NAME OF FUNDING / SPONSORING ORGANIZATION AF Office of Scientific Research 8b. OFFICE SYMBOL (If applicable)	9. PROCUREMENT INSTRUMENT IDENTIFICATION NUMBER
8c. ADDRESS (City, State, and ZIP Code) Bolling AFB, DC 20332	10. SOURCE OF FUNDING NUMBERS PROGRAM ELEMENT NO. 61102F; PROJECT NO. 2303; TASK NO. 2303G2; WORK UNIT ACCESSION NO. 2303G201

11. TITLE (Include Security Classification)
Laboratory Study of Ion-Neutral Collisions at Suprathermal Energies

12. PERSONAL AUTHOR(S)
J. A. Gardner, R. A. Dressler, R. H. Salter, and E. Murad

13a. TYPE OF REPORT	13b. TIME COVERED	14. DATE OF REPORT (Year, Month, Day)	15. PAGE COUNT
Scientific, Interim	FROM 1/88 TO 12/89	1989 December 28	50

16. SUPPLEMENTARY NOTATION

17. COSATI CODES			18. SUBJECT TERMS (Continue on reverse if necessary and identify by block number)
FIELD	GROUP	SUB-GROUP	Ion-neutral collisions, Mass spectrometry, Space effects

19. ABSTRACT (Continue on reverse if necessary and identify by block number)

A double mass-spectrometer system for the study of the dynamics of ion-neutral collisions at suprathermal energies is described in detail. The system consists of a *Wien Filter*, which acts as a source of mass-selected and velocity analyzed ions, coupled to a static-pressure collision chamber followed by a quadrupole mass filter, which acts as a mass analyzer for the products and the projectile ions. This apparatus has been used to measure ion-neutral collision cross sections and ion product times-of-flight. The methods utilized in the processing of raw experimental data are also described. The raw cross section data is corrected with respect to the collection efficiency, yielding integral cross sections which can be used in codes designed to predict the environment of spacecraft in low earth orbit. The performance of the experiment is demonstrated by measuring the known ion-neutral collision systems: $N_2^+ + Ar$, $N_2^+ + D_2$, and $O^+ + H_2O$.

20. DISTRIBUTION / AVAILABILITY OF ABSTRACT	21. ABSTRACT SECURITY CLASSIFICATION
☐ UNCLASSIFIED/UNLIMITED ☒ SAME AS RPT. ☐ DTIC USERS	UNCLASSIFIED
22a. NAME OF RESPONSIBLE INDIVIDUAL RAINER A. DRESSLER	22b. TELEPHONE (Include Area Code) 617-377-2332 — 22c. OFFICE SYMBOL GL/PHK

DD Form 1473, JUN 86 — Previous editions are obsolete.

Preface

This report is a description of the double mass-spectrometer system located in the Spacecraft Interactions Branch Chemistry Laboratory. The apparatus is utilized to obtain cross sections of ion-neutral reactions as well as to study energy partitioning in these reactions. Since its first operation, important modifications have been carried out on the instrument, allowing faster and more accurate data acquisition. These modifications are described in detail.

Contents

Illustrations

Tables

Laboratory Study of Ion-Neutral Collisions at Suprathermal Energies

1. INTRODUCTION

Recent space measurements of the plasma surrounding the Space Shuttle have revealed ionization levels greater than ambient ion densities.[1,2] These mass spectroscopic measurements show that the local environment of the Space Shuttle contains relatively large densities of H_2O^+ and H_3O^+. Since water ions are practically non-existent in the unperturbed atmosphere of low-earth-orbit altitudes (150-400 km), these ions must originate through charge transfer between ambient ions and H_2O.[3,4,5,6] Sources of water vapor include surface outgassing, firing of attitude control jets, and water releases. The ambient ions at orbital altitudes are primarily O^+ ($\approx 99\%$) and N_2^+ ($\approx 1\%$) at a total ion density[7] of about 2×10^5 cm^{-3}.

Collisions between the ambient ions and the contaminant gases surrounding the Shuttle occur at relative velocities related to the Shuttle orbiting velocity of 7.7 ± 0.2 km s^{-1}. The measurements of high water ion densities have renewed the interest in ion-neutral chemistry at suprathermal energies, that is, at energies above 1 eV. Attempts at developing models that predict

---

[1] Narcisi, R. S., Trzcinski, E., Federico, G., Wlodyka, L., and Delorey, D., (1983) *The Gaseous and Plasma Environment Around the Space Shuttle*, AIAA-83-2659, 183.

[2] Grebowsky, J. M., Pharo, M. W., Taylor, H. A., and Eberstein, I. J., (1987) Thermal Ion Perturbations Observed in the Vicinity of the Space Shuttle, *Planet. Space Sci.*, **35**; 501.

[3] Hastings, D. E., Gatsonis, N. A., and Mogstad, T. (1988) A Simple Model for the Initial Phase of a Water Plasma Cloud About a Large Structure in Space, *J. Geophys. Res.*, **93**; 1961.

[4] Caledonia, G. E., Person, J. C., and Hastings, D. E. (1987) The Interpretation of Space Shuttle Measurements of Ionic Species, *J. Geophys. Res.*, **92**; 273.

[5] Hunton, D. E., and Calo, J. M. (1985) Low Energy Ions in the Shuttle Environment: Evidence for Strong Ambient-Contaminant Interactions, *Planet. Space Sci.*, **33**; 945.

[6] Murad, E. (1985) Implications of Mass Spectrometric Measurements on Space Shuttle, *Planet. Space Sci.*, **33**; 421.

[7] Jursa, A., ed. (1985) *Handbook of Geophysics and the Space Environment*, ADA 167000.

the nature of the Space Shuttle orbital environment[3-5,8] require a knowledge of the relevant rate coefficients as a function of energy. An understanding of the energy partitioning in the reaction products is also necessary both to determine the collisional and internal energies at which secondary reactions occur, and to interpret the results from space-borne mass spectrometers whose detection efficiency depends on the ion kinetic energy.

A laboratory program is being conducted by the Spacecraft Interactions Branch to provide data on ion-neutral collisions at suprathermal energies. Under this program, a double mass spectrometer system that was built in the late 1960's[9] is operated. Although the instrument was state-of-the-art at that time, the rapid development of technology mandated various upgrades to improve the accuracy and efficiency of the experiment. These upgrades include a high intensity ion source, faster electronics, a detector with higher efficiency and durability, improved vacuum pumps, and computer automation. The performance of the instrument has been tested using three ion-neutral systems for which reaction cross sections are known: (i) $N_2^+ + Ar$, (ii) $N_2^+ + D_2$, and *(iii)* $O^+ + H_2O$.

In this report we describe the present state of the experiment with emphasis on the most recent modifications. The instrumentation is described in Section 2. The various modes of operation and the methods of raw data analysis are discussed in Section 3. The results for measurements of the above-mentioned reaction systems are reported in Section 4. In Section 5, further improvements for the experiment are recommended. Conclusions are contained in Section 6.

---

[8] Elgin, J. B., Cooke, D. C., Tautz, M., and Murad, E., Modeling of Atmospherically-Induced Gas Phase Optical Contamination from Orbiting Spacecraft, *J. Geophys. Res.*, submitted for publication.

[9] Maier, W. B., and Murad, E. (1971) Study of Collisions between Low-Energy N^+ and N_2: Reaction Cross Sections, Isotopic Compositions, and Kinetic Energies of the Products, *J. Chem. Phys.*, **55**; 2307.

2. INSTRUMENTATION

2.1. Overview of the Apparatus

The laboratory apparatus, shown schematically in Figure 1, consists of a coaxial tandem double mass-spectrometer in a high-vacuum system. In this apparatus, an ion beam is produced

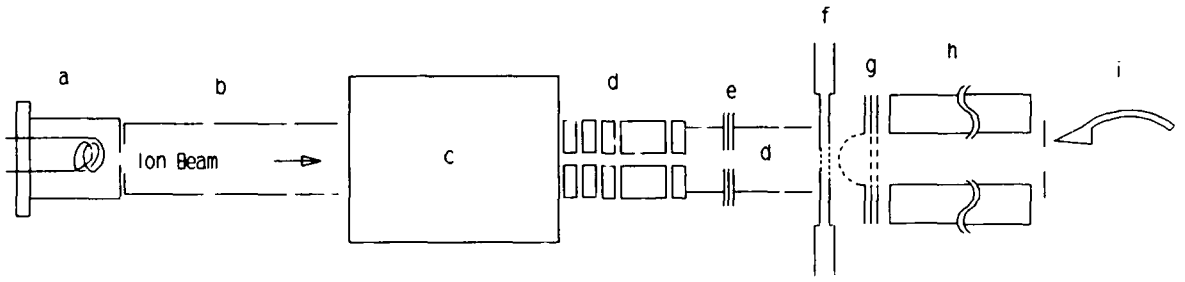

Figure 1: Schematic of Double Mass Spectrometer Apparatus--a) ion source; b) acceleration lens; c) Wien velocity filter; d) deceleration lenses; e) deflector electrode; f) collision chamber; g) collection and acceleration grids; h) quadrupole mass filter; i) channel electron multiplier. Elements are not drawn to scale.

and passed through a static gas cell (the "collision chamber") containing a neutral reactant gas at a typical pressure of about 1 mTorr. The ion beam is formed in either an electron impact or a dc discharge source. The ion beam is accelerated, mass-analyzed in a Wien velocity filter, and then decelerated to control the experimental collision energy. Deceleration occurs in either one or two stages, depending on the final desired energy. The ion beam also passes through a set of "deflector" electrodes, which are used to create a pulsed ion beam in order to conduct ion time-of-flight measurements.

The mass-selected "primary" ion beam passes through the collision chamber which contains the neutral reactant gas. The primary ion beam and the reaction product "secondary" ions emerging from the collision chamber are accelerated towards, and focused onto, the entrance of an ELF quadrupole mass filter. The ions are mass-analyzed in the quadrupole, and those ions selected by the quadrupole are accelerated towards, and detected by, a channel electron multiplier. The

detector output pulses are processed and counted by NIM-module electronics and an AT-compatible computer.

2.2. Ion Source

This apparatus utilizes either of two ion sources: (1) a Colutron Research Corporation Model 101-Q Ion Source that may be operated in either a dc discharge or an electron impact mode; or (2) an electron impact ionization source, designed and built at the Geophysics Lab, similar in design to that of Udseth et al.[10] Design and operational characteristics of each source will be described here.

2.2.1. COLUTRON RESEARCH CORP. ION SOURCE

In the Colutron Research Corporation Model 101-Q Ion Source, electrons are emitted from a spiral tungsten filament (0.05 cm diameter, total length ≈ 3.5 cm) in a quartz enclosed chamber. The pressure within the chamber is approximately 200 mTorr. The source has a molybdenum [Mo] end-plate serving as the anode. In this plate there is an aperture (0.5 mm diameter) through which the source gas effuses into the chamber containing the Wien filter, resulting in a typical pressure of 10^{-5} Torr therein. Electrons from the filament pass through the anode aperture and ionize the effusing source gas, forming the primary ion beam. The entire source is encased in a cooling mantle which is cooled in series with the Wien filter magnet.

As stated earlier, the Colutron source may be operated in either a dc discharge or an electron impact mode. In the dc discharge mode, the anode voltage is initially set to 150 V with respect to the filament potential, and a discharge is struck using high filament emission currents. When the discharge is on, the anode current is typically 0.1 - 0.3 A. Once a discharge has been

---

[10] Udseth, H., Giese, C. F., and Gentry, W. R. (1973) Transition Probabilities and Differential Cross Sections for Vibrational Excitation in Collisions of H^+ with H_2, HD, and D_2, *Phys. Rev. A*, 8; 2483.

established, the anode voltage is reduced to the lowest possible level while still maintaining a discharge, typically 50 V. This setting determines the energy of the electrons that ionize the source gas. In order to operate the Colutron source at electron energies below 50 eV, the electron impact mode is used. To operate in this mode, the anode voltage is set to 20 - 30 V and the filament current is set below discharge conditions. Under these conditions, the anode current is less than 10 mA.

The Colutron source produces typically 5×10^5 to 2×10^6 primary ions per second in the discharge mode, but only 5×10^3 to 2×10^4 ions per second in the electron impact mode. The high discharge mode signal levels exceed the specified maximum count rates of the detection electronics unless the Wien filter is detuned to attenuate the signal; while the electron impact mode signal is insufficient to perform time-of-flight measurements. The Colutron source operates at a power level of about 400 - 600 Watts regardless of which operational mode is in use. These high power levels typically cause filament burn-out in 60 hours of operating time. Also, tungsten vapor is deposited on all surfaces inside the ion source during source operation, eventually causing short circuits and requiring replacement of all source parts.

2.2.2. ELECTRON IMPACT IONIZATION SOURCE

Ideally, experiments should be performed at the lowest electron energy at which a usable ion current is produced, to minimize the production of long-lived electronically excited ion states. The ion beam intensity increases significantly as the electron energy is increased above the appearance potential of the ion. For gases used in this study, the appearance potentials are between 15 and 25 eV. The discharge source is not stable at anode potentials below about 50 V. Also, the ion currents are very low when the Colutron source is operated in the electron impact mode. Consequently, a second source (the "EI source") similar to that of Udseth et al.[10] was designed and built at the Geophysics Laboratory.

The EI source is designed to fit into the cooling mantle of the Colutron source. The anode is a molybdenum tube (0.91 mm inside, 1.52 mm outside diameter) through which the source gas is passed. The Mo tube is inserted into a ¼ inch o.d. ceramic tube for insulation and vacuum feedthrough purposes. The filaments in this source are two strips of either 1%-thoriated tungsten or thoriated iridium ribbon (each strip is about 1.5 cm long by 0.08 cm by 0.005 cm). The filaments are positioned about 0.3 cm downstream of the anode tip through which the source gas is emerging. Ions are produced at the Mo tube exit and are accelerated in the direction of the filaments. Following the filaments is a Mo endcap plate with a small aperture (0.5 mm diameter) forming the exit aperture of the source region. This plate is biased to the more negative side of the filament power supply. Ions passing through the aperture form the primary ion beam. The EI source is generally tunable to reach signal levels from 2×10^4 to 4×10^5 primary ions per second, permitting operation at levels both (a) lower than the saturation limit of the detection electronics, and (b) large enough to perform both reaction cross section and time-of-flight measurements under identical source conditions.

The source backing pressure (about 200 mTorr) in the EI source is comparable to that in the Colutron source. The pressure drop in the EI source occurs primarily along a long, narrow tube (the Mo tube anode and the ceramic tube which holds and insulates the Mo tube). The pressure in the region between the Mo tube and the endcap aperture is less than 10^{-3} Torr and may be nearly as low as the Wien filter chamber pressure of about 10^{-6} Torr. The main pressure drop in the Colutron source, however, occurs across the 0.5 mm diameter aperture in the source end-cap. Consequently, the gas flux through the EI source is approximately one order of magnitude lower than through the Colutron source. There are two important results of this lower gas flux: (1) the pressure in the high vacuum side of the ion source is about one order of magnitude lower when using the EI source--this reduces the probability of a collision between a primary ion and a background gas molecule in the high vacuum source region; and (2) since much less source gas is

used to operate the EI source, experiments with expensive isotopically labelled gases (such as $D_2{}^{18}O$) are more economically feasible.

Finally, the EI source operates typically at 30 Watts, with a maximum power of about 45 Watts. This is an order of magnitude less power than that used by the Colutron source. The filament lifetime in the EI source is approximately twice as long as in the Colutron source.

2.3. Primary Beam Optics

The primary beam is accelerated to 150 Volts upon exiting the source. The ion beam enters a Colutron Research Corp. Wien velocity filter that preferentially passes ions of one set mass-to-charge ratio (for example, 28 atomic mass units [a.m.u.] to produce an $N_2{}^+$ beam). In the Wien filter the ion beam, a magnetic field, and an electric field are mutually orthogonal. The Wien filter fields are tuned so that the ion beam will be deflected in one direction by the magnetic field, but the opposite direction by the electric field. This results in ions of the selected mass being passed undeflected through the filter, while ions having different masses are rejected by the filter. The Colutron Wien filter is equipped with tapered magnet pole plates, as well as fourteen electrostatic guard rings that are adjusted to shape the magnetic and electric fields to minimize focusing of the beam by the Wien filter.[11]

Following the Wien filter, the mass-selected beam is decelerated to a minimum of 20 eV using an einzel lens (Colutron Research Corp.). The ion beam then passes through the ion pulsing manifold, which is described below. After this manifold, the ion beam passes through a second lens stack, designed and constructed at the Geophysics Laboratory, which may be used to further reduce the ion beam energy.

The second lens stack was added to improve the primary ion beam intensity at the collision chamber. Prior to adding this second lens stack, the entire ion retardation was performed with the

---

[11] Wahlin, L. (1964) The Colutron, a Zero Deflection Isotope Separator, *Nuclear Instruments and Methods*, **27**; 55.

Colutron einzel lens. The ion beam then passed through the deflecting manifold, and next traversed a region approximately 11.4 cm long, prior to entering the collision chamber. A cylindrical screen, which was floated at the collision chamber potential, surrounded this region to keep the region field-free. At low ion energies ($E_{beam} \leq$ 10 eV) the ion beam intensity was greatly reduced due to the increase in beam divergence as the deceleration voltage ratio increased. To minimize the loss of ions, it is preferable to retard the ion energy as late as possible in the apparatus. With the second lens stack, the ion beam is decelerated within about 3 cm of the collision chamber entrance, rather than the previous distance of 11.4 cm. Using this two-stage deceleration greatly enhances the primary intensity in experiments using low energy primary ions.

The second lens stack consists of three separately regulated elements. The first element follows the final element in the Colutron einzel lens and these two elements are held at the same potential. The difference between this potential and the collision chamber potential determines the second deceleration potential applied to the ion beam. The second and third elements, which are 6.0 and 3.1 cm long, respectively, are tuned to maximize the primary beam intensity. The applied potentials have been analyzed using the SIMION ion trajectory program[12].

To obtain reliable cross section data, focusing of the primary beam in the collision chamber must be avoided. Such focusing results in a divergent beam exiting the collision chamber, causing primary ion losses at the quadrupole exit. To obtain a beam as near parallel as possible at the collision chamber, the primary beam is maximized by first setting *all* grids following the collision chamber to ground, then tuning the source and decelerator focusing elements. The focusing elements following the collision chamber are then adjusted to collect all of the primary ions that pass through the collision chamber.

---

[12] Dahl, D. A., Delmore, J. E., and Appelhaus, A. D. (1990) SIMION PC/PS2 electrostatic lens design program, *Rev. Sci. Instrum.*, **61**; 607.

2.4. Ion Pulsing Manifold

The ion pulsing manifold consists of a set of deflector plates, which may be used to steer the primary ion beam away from the collision chamber entrance aperture. These plates are shown schematically in Figure 2.

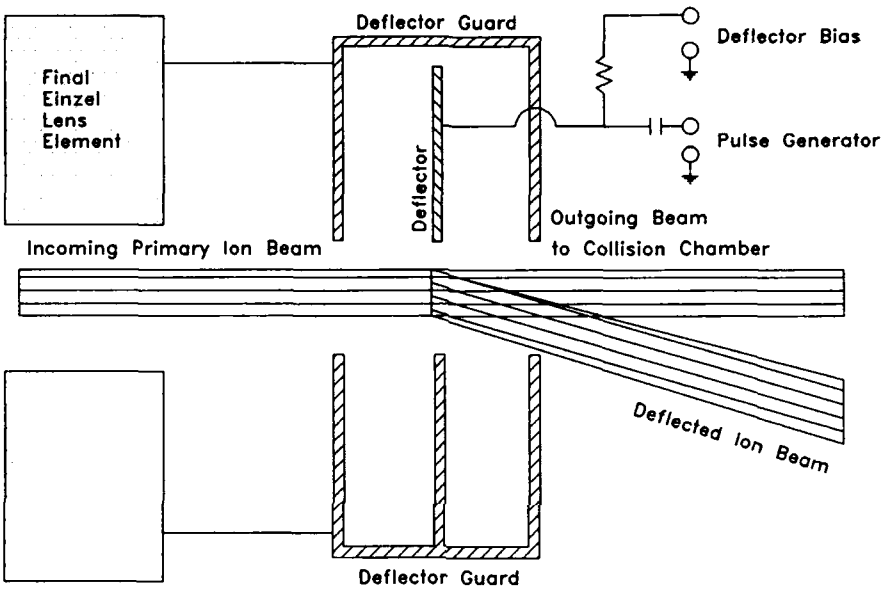

Figure 2: Schematic of Ion Beam Deflection Region.

When the *deflector* potential is held close to the *deflector guard* potential, the primary ion beam passes through the electrodes to the collision chamber. By setting the *deflector* potential to a higher voltage than the *deflector guard* potential (applying a *holdoff potential*), an electric field is created that deflects the ion beam. This holdoff potential is typically 20 V, while the deflector guard potential is biased at the potential of the last einzel lens element.

For time-of-flight measurements, this holdoff potential is applied to the deflector electrode to deflect the beam so that it does not pass into the collision chamber. Ion pulses are produced by coupling a negative voltage pulse to the deflector bias potential via a high pass filter (see Figure 2). This "gate pulse" is equal in magnitude to the holdoff potential with a 10 to 20 kHz

repetition rate and a pulse width of 1 to 3 microseconds. These pulses are shown schematically in Figure 3.

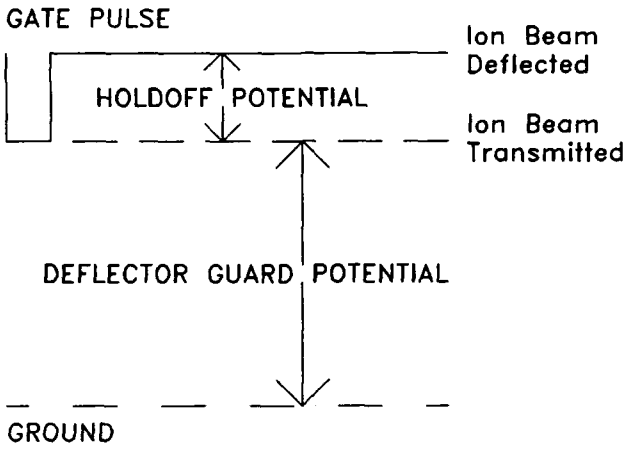

Figure 3: Schematic of Potentials Applied to Deflector Electrode in a Time-of-flight Experiment.

2.5. Collision Chamber

The collision chamber, shown in Figure 4, is 0.27 cm long and contains the target gas at a typical static pressure of 1 mTorr. The chamber has two ¼-inch (o.d.) gas ports: (1) a gas inlet

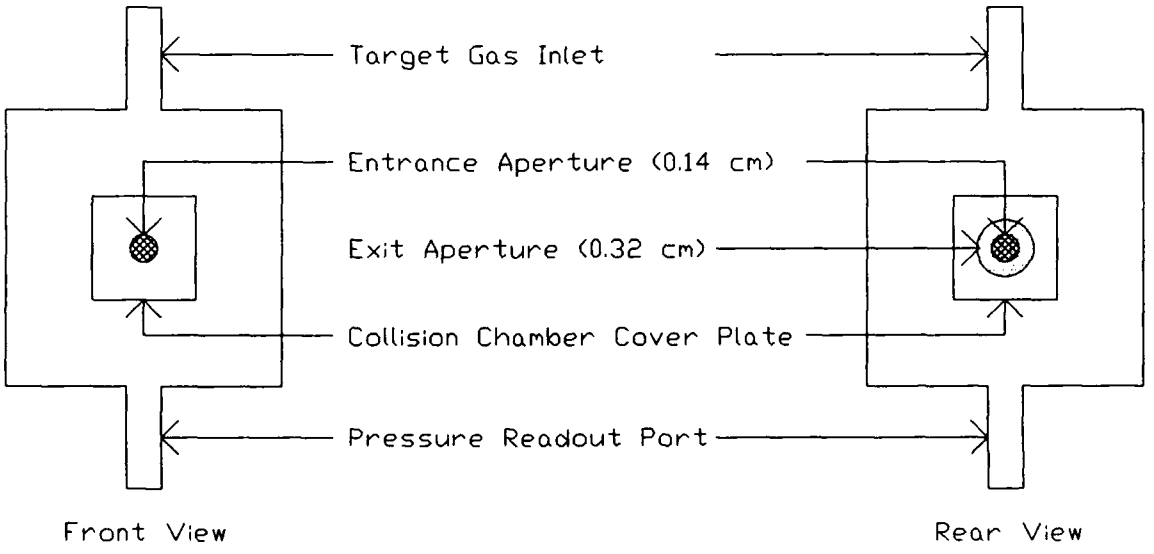

Figure 4: Schematic of the Collision Chamber.

for the target gas; and (2) a port connecting to a pressure gauge (MKS Baratron Model 390HA, 1 Torr full range, absolute pressure readout). The entrance and exit apertures for the ion beam are 0.14 and 0.32 cm diameter, respectively. These apertures are covered with a fine mesh gold grid (78 percent transmission, 200 lines per inch) to minimize leakage into the chamber of external electric fields. The grids also provide a sharp boundary for the pressure drop-off between the collision chamber pressure and that of the high-vacuum region ($\approx 3 \times 10^{-6}$ Torr) that surrounds the collision chamber. The entire collision chamber has been gold-plated to provide an inert surface with a uniform potential throughout the chamber.

2.6. Acceleration Optics

The ions exiting the collision chamber are accelerated towards and focused into the entrance of the quadrupole mass spectrometer by a series of three grids shown in Figure 1. The first grid is hemispherical, while the second and third grids are flat and perpendicular to the experimental axis. The hemispherical grid potential is adjusted for focusing, while the second and third ("final") grids are held at ground, the quadrupole potential. As will be discussed, a potential may be applied to the final grid to measure the energy of the primary ions.

During a typical cross-section measurement, the potential difference between the collision chamber and the quadrupole is about 80 V. The potential applied to the hemispherical grid is varied to maximize the throughput of the primary *and* the secondary ions; this potential is typically about 40 V.

During time-of-flight experiments, the potential difference between the collision chamber and the quadrupole is approximately 20 V. The potential applied to the hemispherical grid is regulated to give a difference between the collision chamber and the hemispherical grid of 20 mV. In this manner, the path length over which the ions are at low energy in a (nearly) field free region is increased, so that the energy resolution for the time-of-flight is improved. The small potential (20 mV) is applied so that secondary ions formed with near-zero energy (laboratory frame) are

accelerated slightly to overcome the barriers due to surface potentials that may be present on the hemispherical grid.

2.7. Secondary Mass Analysis

The second mass spectrometer is an ELF quadrupole mass filter (Extrel Corp.). The quadrupole consists of four parallel rods, 20 cm in length, which are arranged in a square pattern. A dc and (high voltage) radio frequency potential is applied to the poles such that adjacent poles are 180° out of phase. Only ions with a selected mass-to-charge (m/e) ratio have stable trajectories through the quadrupole region.[13] Ions with other values of m/e will have unstable trajectories and will strike the rods, where the ions are neutralized. The quadrupole chamber pressure is maintained at typically 6×10^{-8} Torr by a CTI Cryogenics Model 7 cryopump.

2.8. Ion Detector and Counting Electronics

Ions that have passed the quadrupole are accelerated by a 2000 V potential applied to the cathode of a channel electron multiplier (Galileo Electro-Optics Corp.). Channel electron multipliers are heavily lead-doped, horn shaped glass tubes with secondary emissive and resistive characteristics. In contrast to the more traditional discrete-dynode electron multipliers containing several dynodes, the channel electron multiplier consists of a single continuous dynode surface within the glass tube. A potential applied across the tube will result in a continuous voltage gradient within the tube. Secondary electrons are produced by ions striking the surface and are accelerated within the tube, gaining energy that enables these electrons to create further secondary electrons upon hitting the channel surface.

---

[13] See for example: Paul, W., and Steinwedel, H. (1953) Ein neues Massenspektrometer ohne Magnetfeld, *Z. Naturforsch*, **8a**; 448; Paul, W., and Raether, M. (1955) Das elektrische Massenfilter", *Z. Physik*, **140**; 262; Paul, W., Reinhard, H. P., and von Zahn, U. (1958) Das elektrische Massenfilter als Massenspektrometer und Isotopentrenner, *Z. Physik*, **152**; 143.

In recent years, channel electron multipliers have widely replaced discrete-dynode electron multipliers. The most important advantages of channel electron multipliers are: low dark count rates; a stable dynode surface that is insensitive to atmospheric exposure; narrow gain distribution of output pulses; lower bias voltages and currents; and smaller physical size. Channel electron multipliers have typical ion detection efficiencies ranging between 80 and 100 percent, depending on the mass of the ion[14,15]. The multiplier in this work is a high current Channeltron that can be operated in either a pulse counting or analog mode. The detector generates pulse heights greater than 100 mV. This signal is passed through a 300 MHz preamplifier (Stanford Research Systems, Inc.) to modify the impedance. The counting electronics consist of a 120 MHz 10:1 amplifier (EG&G Ortec); a 100 MHz signal discriminator (EG&G Ortec) capable of rejecting spurious signals picked up in the signal chain; a ratemeter (Mechtronics Nuclear) and a scaler-timer (Ashton) to monitor the signal level; a Davidson time-to-digital conversion unit which is used to conduct time-of-flight measurements; and a Zenith Z-248 AT-compatible microcomputer, outfitted with two Metrabyte data processing plug-in modules.

2.9. Data Acquisition

In the last ten years, the microcomputer has become an indispensable tool in the laboratory. Due to their low cost and versatility, microcomputers have in many instances replaced sophisticated microprocessor based equipment used for the acquisition, storage, and processing of experimental data. The interface between an experiment and a microcomputer requires a minor investment in interface hardware and software. Due to the simplicity of basic digital electronics, it is possible to design and build an interface computer plug-in card in the laboratory. Indeed, in the earlier stages

---

[14] Burrous, C. N., Lieber, A. J., and Zaviantseff, V. T. (1967) Detection Efficiency of a Continuous Channel Electron Multiplier for Positive Ions, *Rev. Sci. Instr.*, **38**; 1477.

[15] Potter, W. E., and Mauersberger, K. (1972) Spiral Electron Multiplier Operation Characteristics Using Positive Ions, *Rev. Sci. Instr.*, **43**; 1327.

of personal computer (PC) history, this was frequently the best option.[16] In recent years, however, easy-to-program interface cards have been mass-produced and marketed for many laboratory applications. Although commercial interface software is increasingly available and frequently sold with appropriate hardware, the versatility of commercial software is often limited. In many cases, the vendors do not provide the source code with the package. In cases where the source code *is* available, it is often difficult to modify, due to poor documentation or the use of obscure program compilers or language variations. Consequently, the versatility of microcomputer based data acquisition is significantly enhanced if the acquisition software is generated by the user.

We have interfaced our instrument to an AT-computer using a system co-developed with Michael Allan of the University of Fribourg, Switzerland. The first version of this system is described in Reference 16. The hardware, consisting of 2 commercial interface cards and additional external electronics, is described in Section 2.9.1. The software is briefly outlined in Section 2.9.2.

2.9.1. HARDWARE

The basic hardware components necessary to successfully control an experiment with a computer are:

1. Signal processing electronics
2. Computer input interface
3. Computer with sufficient speed and available RAM (random access memory)
4. Experiment control interface
5. Display device

The hardware configuration of the present experiment is shown in Figure 5. The signal processing electronics transform the pulses generated by the Channeltron detector to TTL pulses.

---

[16] Dressler, R., Gremaud, M., Chassot, P.-H., and Allan, M. (1985) The Control of a Negative Ion Mass Spectrometer by an Apple II Computer: A Versatile Interface Card for Control of Chemical Instrumentation, *Chimia*, **39**; 327.

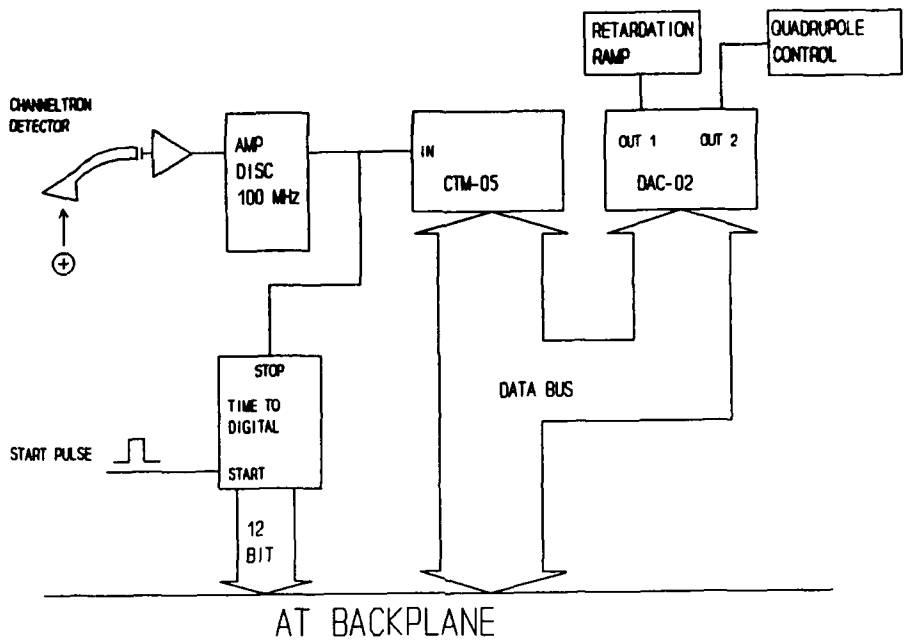

Figure 5: Schematic of the Data Acquisition System.

When the experiment requires the determination of an ion count rate, the TTL output of the discriminator is fed directly to the computer input interface (Metrabyte CTM-05). The signal line is connected to the input of one of five counter-timers. A timer is programmed to produce a constant square wave signal that is connected to the count-enable gate of the signal counter. The length of the count-enable pulse (dwell time) is predetermined by the user and is well defined. The microprocessor has access to latches in the counters, from which the data can be read.

When measuring time intervals between events, as in time-of-flight measurements, the TTL signal is connected to the STOP input of a time-to-digital converter. The time-to-digital converter initiates counting of an adjustable clock signal after receiving a pulse at the START input. When a stop pulse is received, the current counter value is latched. The computer then reads the 12-bit data corresponding to the time interval via a parallel port.

If the experiment requires scanning of the mass filter or of a retardation electrode, a digital ramp must be incremented between count periods. The experimental control interface in this case is a 12-bit digital-to-analog converter (DAC) (Metrabyte DAC-02) with output range 0 to ± 10 V.

The output of the DAC may be connected to a programmable power supply to provide larger voltage scan ranges.

A Zenith model ZVM-1380-C enhanced graphics adapter (EGA) color monitor is used to provide a real-time display of experimental data.

2.9.2. SOFTWARE

The role of the software is to:

1. Accept the data acquisition parameters and control commands of the user.
2. Read the counter in multichannel scaling (MCS) or the digital input in time-of-flight (TOF) mode. In the MCS mode, the result is added into an array of consecutive memory locations (channels). In the TOF mode, the content of the channel corresponding to the digital input is incremented.
3. Control the experiment by setting the analog output voltages to appropriate values.
4. Display the experimental data during acquisition.
5. Store the complete data onto a disk.
6. Manipulate the data and create hard copies.

The main code is written in FORTRAN 77, while MACRO ASSEMBLER is used to control the interface cards, and color graphics routines are written in C. The main program consists of the command menu, the main acquisition routines, and various spectrum manipulation and option setting routines. It also controls the loading and saving of experimental data (spectra), which are stored as binary files containing acquired data and acquisition parameters. Special routines include on-screen calculation of ion-neutral collision cross sections from recorded mass spectra and conversion of the time-of-flight scale to laboratory energy of product ions.

The counter-timer card must be initialized by reading specific code numbers to various registers. This is accomplished using an ASSEMBLER routine. When data is read from the counters, the FORTRAN program calls an ASSEMBLER routine which carries out the machine

level operation. In the TOF mode, the 12-bit output of the time-to-digital converter is read through the parallel ports. An ASSEMBLER routine also controls the output of the digital to analog converters.

3. MEASUREMENT MODES

3.1. Overview

In this section, we describe the types of experiments that are performed using the double mass spectrometer. Experiments include:

1. Primary ion beam retardation scans, which are performed to determine the energy of the primary ions
2. Cross section measurements, in which the quadrupole mass spectrometer is scanned over a short range of masses including the primary ion and the possible reaction product masses. Measurement of the signal intensities for the primary and product ions leads to the determination of the reaction cross sections.
3. Time-of-flight measurements, performed on both the primary and secondary ions to determine the energies of the ions.

3.2. *Primary Beam Retardation Scans*

In each experiment, it is imperative that the energy of the primary ions be known. This energy is measured by monitoring the primary ion signal while ramping a potential on the final grid between the collision chamber and the quadrupole. As the potential on this grid is increased, the primary signal decreases due to ion rejection by the electric field produced between the final grid and the grounded second grid. The ions are stopped from passing through the grid when the potential applied to the final grid is equal to the ion energy. At this point, as shown in Figure 6 (solid line), a sharp falloff occurs in a plot of the ion intensity versus applied retardation voltage. The maximum slope is taken to be the average primary ion beam energy. The uncertainty in the ion beam energy is taken to be the average energy difference between the measured ion beam energy and the energies corresponding to the points where 10 percent and 90 percent of the beam is attenuated [relative to the ion intensity at the energy where the sharp falloff begins]. The accuracy of the energy determination is increased by calculating the first derivative of the smoothed

retardation plot (shown by the dashed line in Figure 6). The minimum in the first derivative curve corresponds to the maximum slope in the retardation plot.

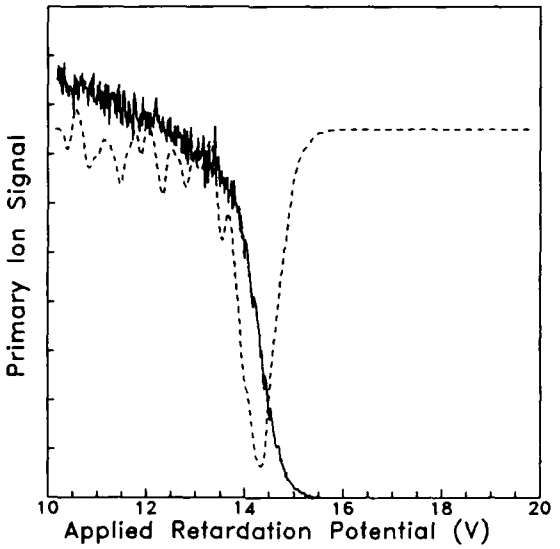

Figure 6: Typical Retardation Scan (Solid) to Determine Primary Ion Energy, Which for This Case is 14.3 ± 0.5 eV N_2^+. The first derivative of this curve is also shown (dashed).

3.3. Cross Section Experiments

3.3.1. CROSS SECTION METHOD

Before performing an experiment to determine a reaction cross section, a target gas pressure of 0.5 to 1 mTorr is established; the quadrupole mass resolution and the detector bias voltage are adjusted so that mass-dependent discrimination is negligible; and a retardation scan is recorded to determine the energy of the primary ions. The quadrupole mass spectrometer is then scanned over a mass-to-charge ratio range that enables the observation of singly-charged primary and possible secondary ions. The scan is performed over a 20 to 40 a.m.u. range, dwelling for 10 msec each on 256 incremental steps. Adequate signal-to-noise ratios are typically obtained by accumulating 100 such scans.

A typical mass spectrum is shown in Figure 7 for a reaction between N_2^+ and D_2O. The primary N2+ signal is shown by the solid line, while the points represent data that has been multiplied by a factor of 100 to show the signals corresponding to the product ion masses (a.m.u. 20 for D_2O^+ and a.m.u. 30 for N_2D^+).

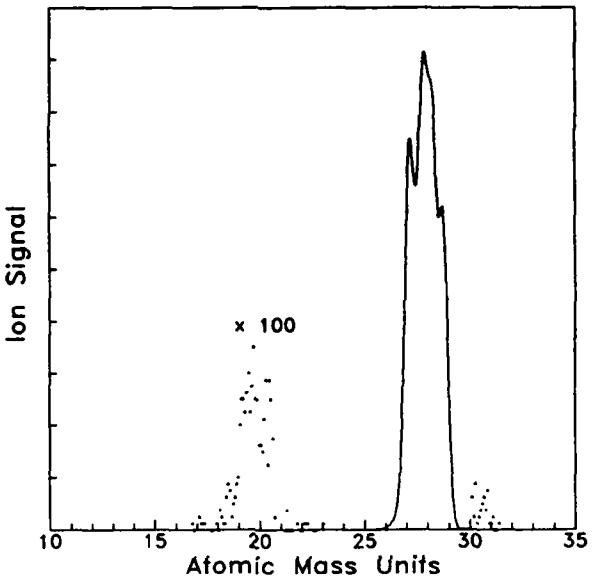

Figure 7: Typical Mass Spectrum to Determine Reaction Cross Section. Solid line shows data for primary ion (N_2^+); points show data for product ions (D_2O^+, N_2D^+) multiplied by 100.

The observed reaction cross section is calculated by first integrating the signals corresponding to the primary and secondary ions, designated I_{prim} and I_{sec} respectively. To integrate, one sums the contents of the channels associated with each ion. The ratio of the secondary to primary ion signals follows a Beer's Law proportionality to the reaction cross section

$$\frac{I_{sec}}{I_{prim}} = \sigma_{exp}\, l\, n \qquad (1)$$

where σ_{exp} is the experimentally observed reaction cross section, l is the interaction length, and n is the target gas concentration. The number of secondary ions produced, and thus the attenuation of the primary ion beam, is typically less than 0.1 percent of the number of primary ions. The linear approximation to Beer's Law is therefore sufficient for our analysis.

Equation (1) is rearranged to solve for σ_{exp} and, for the specific case of this experiment, l = 0.27 cm; P, the target gas pressure, is in units of Torr; and σ_{exp} is in units of cm^2:

$$\sigma_{exp} = 1.14 \times 10^{-16} \left(\frac{1}{P}\right) \left(\frac{I_{sec}}{I_{prim}}\right) . \qquad (2)$$

Typical cross sections obtained in this work are on the order of 10^{-16} cm^2 (1 $Å^2$).

The observed reaction cross section is equal to the integral reaction cross section only when the collection efficiencies for the primary and secondary ions are identical. As will be shown, in our experiments this criterion is met by reactions in which the secondary ion velocity distribution is strongly forward peaked. Such a reaction occurs between N_2^+ and D_2;[17] our results for this reaction pair will be discussed in Section 4.

In cases where the collection efficiencies are different for the primary and secondary ions, an integral reaction cross section may still be calculated provided the relative collection efficiencies are known. One possible source of discrepancy in the relative collection efficiencies is poor focusing of the ions into the quadrupole. Extensive study has shown that when the potential on the hemispherical grid is approximately one-half of the collision chamber bias voltage, both the primary and secondary ion collection efficiencies are maximized. In each experiment, the hemispherical grid potential is therefore adjusted to maximize the primary ion signal. The quadrupole resolution is adjusted so that essentially 100 percent of the ions entering the quadrupole will be passed to the detector when those ions are mass selected by the quadrupole.

In many reactions, secondary ions are scattered at large angles in the laboratory frame. Consequently, the secondary ion collection efficiency may be significantly smaller than that of the primary ion beam. In the following section, the problem of determining the secondary ion collection efficiency is discussed.

---

[17] Turner, B. R., Fineman, M. A., and Stebbings, R. F. (1965) Crossed-Beam Investigation of N_2D^+ Production in N_2^+-D_2 Collisions, *J. Chem. Phys.*, **42**; 4088.

3.3.2. CALCULATION OF COLLECTION EFFICIENCY

At collision energies above 1 eV, ion-neutral reactions frequently occur with very little momentum transfer. Consequently, the velocity distribution of the product ions is often found to be similar to that of either the primary beam or the target gas. When the product ion velocity distribution is similar to the primary ion distribution, the product ions are collected efficiently and an integral cross section is determined.

When the ionic product velocity distribution is closely related to the target gas motion (as is frequently the case in charge transfer reactions), a near-thermal velocity distribution is found. These secondary ions are isotropically scattered in the laboratory frame; thus, only a fraction of the product ions exit the collision chamber and can be detected. The measured cross section therefore represents a partial cross section, accounting only for the ions scattered into a composite solid angle $d\omega$ given by the collision chamber dimensions. If the product ions are found to be scattered isotropically in the laboratory frame, the integral cross section can be obtained by calculating this solid angle $d\omega$ throughout the interaction region.

This case is demonstrated in Figure 8, in which are shown schematically the entrance and exit apertures of the collision chamber with diameters d_{in} and d_{ex}. The dashed lines indicate the volume of the collision chamber in which ions are formed, provided the ions travel parallel to the z-axis. Ions produced at a point P(x,y,z) exit the collision chamber in the direction of the quadrupole mass filter if they are scattered within the solid angle ω. By definition of solid angle, ω is proportional to the sphere surface segment A with a base circle of radius b. The radius r of the sphere is the longest distance between P(x,y,z) and the exit aperture edge and is given by

$$r = [\{c - z\}^2 + \{(x^2 + y^2)^{0.5} + r_{ex}\}^2]^{0.5} \qquad (3)$$

where c is the distance between the apertures and $r_{ex} = \frac{1}{2}d_{ex}$. The surface A is given by

$$A = 2\pi r\{r - (r^2 - b^2)^{0.5}\} \qquad (4)$$

and b is given by

$$b = 0.5\{(d_{ex} + d')^2 + (c')^2\}^{0.5} \qquad (5)$$

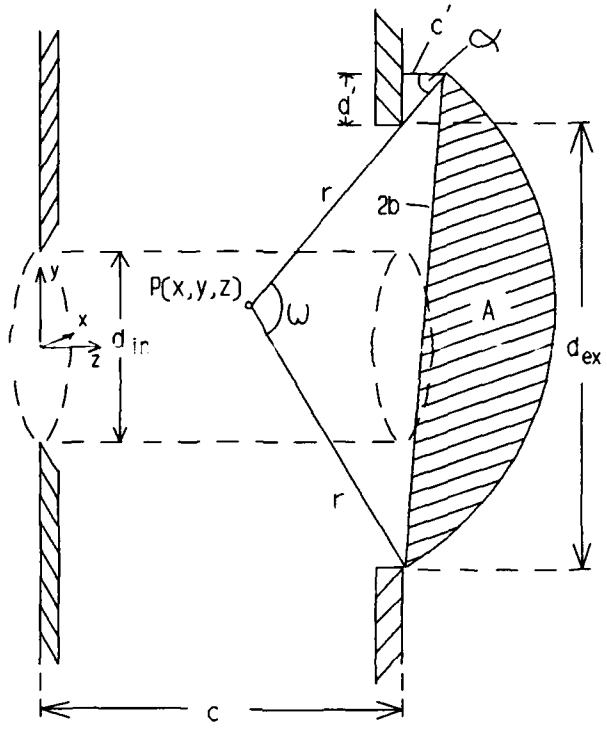

Figure 8: Collision Chamber Area Including the Parameters Used in Calculating the Collection Efficiency.

where the distances d′ and c′ are shown in Figure 8. The distance d′ is given by

$$d' = (r \sin\alpha) - \{r_{ex} - (x^2 + y^2)^{0.5}\} \qquad (6)$$

where α, which is also shown in Figure 8, is given by

$$\tan\alpha = \frac{r_{ex} - (x^2 + y^2)^{0.5}}{c - z} \qquad (7)$$

and c′ is given by

$$c' = (r \cos\alpha) - (c - z) . \qquad (8)$$

The fraction of isotropically scattered ions produced at point P(x,y,z) which pass through the exit aperture is given by the fraction between the sphere segment surface A and the entire sphere surface

$$\eta_i = A_i / 4\pi r_i^2 . \qquad (9)$$

The total collection efficiency of isotropically scattered ions, η, is then obtained numerically by adding and averaging the collection efficiencies at an infinite number of equally distributed points in the collision volume

$$\eta = (1/N) \sum_{x} \sum_{y} \sum_{z} \eta_{xyz} \qquad (10)$$

where N is the total number of points evaluated in the numerical calculation. The accuracy of the calculation depends on the density of points P(x,y,z). The collection efficiencies η are calculated as a function of the grid spacing on the three dimensional grid that spans the point space. The results of these calculations are presented in Table 1. From the calculations it is seen that the effective collection efficiency converges to 20.8 ± 0.1 percent. When the angular distribution of the ionic reaction products is isotropic in the laboratory frame, the integral cross section (σ) is

$$\sigma = \sigma_{exp}/\eta = \sigma_{exp} \times 4.81 \, . \qquad (11)$$

It will be shown in a later section that the use of the correction factor in Eq. (11) provides very good agreement with reported results from other experiments, provided the ionic products are scattered isotropically.

Table 1. Calculated Collection Efficiency of Isotropically Scattered Products as a Function of Point Volume Integration Step.

Integration step (mm)	Collection Efficiency (%)
0.2	20.3
0.1	21.1
0.07	20.5
0.05	20.8
0.03	20.8
0.01	20.7
0.005	20.8

3.4. Time-of-flight Experiments

3.4.1. TIME-OF-FLIGHT METHOD

In addition to obtaining reaction cross section data, it is important to measure the kinetic energy of the reaction product ions. This information is needed (1) to deduce information about internal excitation of the products; (2) to understand possible secondary reactions in the Space Shuttle orbital environment; and (3) to determine the detection efficiencies of the product ions by space-borne mass spectrometers. Ion time-of-flight measurements provide information on the kinetic energy of the product ions.

Time-of-flight measurements are performed by pulsing the primary ion beam (as described in Section 2.4). A Stanford Research Digital Delay generator provides a timing pulse (10 to 20 kHz) to a variable power supply (Chronetics, Inc., PG-13A). This power supply provides the gate pulse, with both variable amplitude (typically 20 V) and duration (1 to 3 microseconds). The Digital Delay generator also provides the "START" pulse to the time-to-digital converter which receives a "STOP" pulse from the amplified, discriminated output of the Channeltron detector. The time-of-flight unit is typically set for 256 channels, with 160 nanoseconds per channel, giving a total time-of-flight window of about 41 microseconds. The start pulse is delayed so that both the primary ion pulse and the secondary ions will appear during the time-of-flight window.

While performing time-of-flight experiments, the collision chamber is floated at about 20 V relative to the quadrupole. As described in Section 2.6, the hemispherical grid is floated to be about 20 mV lower in potential than is the collision chamber so that any product ions with near-zero energy (laboratory frame) will be slightly accelerated to overcome any spurious surface potentials which may exist on the grids. Floating the hemispherical grid at nearly the collision chamber potential increases the drift path for the ions, while maintaining the usefulness of the hemispherical grid as a focusing element. The drift path is the region in which the ions drift prior to being strongly accelerated towards the detector. The resolution of the ion energy determination by the time-of-flight method increases as the drift path length is increased.

3.4.2. ENERGY DETERMINATION

Time-of-flight experiments are performed on both the primary ion beam and the secondary reaction product ions. Measuring the time-of-flight of the primary ion beam serves as a cross-check for the results of the retardation scans in which the primary ion beam energy is measured. Using the known system dimensions and applied potentials along with the measured electronic delays in the detection system, one may calculate the primary ion beam energy from the time-of-flight using basic electrostatic equations.[18] The beam energy calculated in this manner is in very good agreement with the energy measured by the retardation scans.

The laboratory frame kinetic energy of the secondary ions is calculated from the time-of-flight data. In this case, the measured time-of-flight consists of the time required for the *primary* ions to traverse the distance from the deflector to the point in the collision chamber at which a collision occurs, *plus* the time required for the *secondary* ions to traverse the path from that point in the collision chamber to the detector (plus electronic delays in the detection system). In order to calculate the secondary ion energy, the time (τ_p) required for the *primary* ions to travel from the collision chamber center to the detector is first calculated, using the known primary ion energy obtained from a retardation scan. The τ_p is subtracted from the peak value from the primary ion time-of-flight, yielding τ_{ar}, the "arrival time" of the primary beam at the collision chamber center. This τ_{ar} is actually the sum of the time required for the primary beam to 'arrive' at the collision chamber center *plus* the electronic delay in the detection system. When τ_{ar} is subtracted from the time-of-flight data for the secondary ions, the result is simply the time-of-flight from the collision chamber center to the detector for the secondary ions. Using this time and the known potentials and system dimensions, we calculate the laboratory frame kinetic energy of the secondary ions. These calculations are included in the computer data acquisition program, so the secondary ion energies may be calculated immediately after completing a time-of-flight spectrum.

---

[18] Paulson, J. F., Dale, F., and Studniarz, S. A. (1970) Study of Ion-Neutral Reactions with a Time-of-Flight Double Mass Spectrometer, *Intl. J. Mass Spec. and Ion Phys.*, **5**; 113.

4. RESULTS AND DISCUSSION

The experimental apparatus in its current configuration is designed to provide information regarding cross sections and product kinetic energy release of ion-neutral reactions. To test the performance of this apparatus, experiments have been performed to measure three known reactions:

$$N_2^+ + D_2 \rightarrow N_2D^+ + D \qquad [1]$$

$$O^+ + H_2O, D_2O \rightarrow O + H_2O^+, D_2O^+ \qquad [2]$$

and $$N_2^+ + Ar \rightarrow N_2 + Ar^+ \qquad [3].$$

Reaction [1] is known to proceed via a "spectator stripping" mechanism at suprathermal collision energies,[17] resulting in a strongly forward-peaked (laboratory frame) product ion velocity distribution. Primary and secondary ions are therefore detected with almost equal efficiency in this reaction. Comparison of our measured cross sections for Reaction [1] to those reported in Reference 17 provides a good check on the parameters used to determine the cross sections, such as target gas density and effective interaction length.

As will be shown, the charge transfer product ions from Reaction [2] exhibit a near-thermal laboratory energy at collision energies above 2 eV. This indicates that these ions have an isotropic velocity distribution in the laboratory frame. The cross sections for Reaction [2] have been measured in an Ion Cyclotron Resonance (ICR) experiment[19]. The cross sections reported from such an experiment are true integral cross sections. This reaction can therefore be used to check the accuracy of our collection efficiency calculation in the case of isotropically scattered product ions.

In order to obtain the best information on the state-to-state dynamics of an ion-neutral reaction, the primary ion internal energy distribution must be as well-defined as possible. Usually

---

[19] Heninger, M., Fenistein, S., Mauclaire, G., Marx, R., and Murad, E. (1989) Review of the Reaction of O^+ with H_2O and Its Bearing on Composition Measurements from the Space Shuttle, *Geophys. Res. Lett.*, **16**; 139.

one attempts to obtain primary ions in the ground electronic and vibrational state. In most cases the electronic ground state of the primary ion can be selectively populated simply by controlling the ionizing potential to be only slightly above the appearance potential. One thus avoids production of long-lived metastable ions. It is not always possible, however, to perform experiments with such low ionization energies due to the corresponding low ion currents produced when the ionization energy is near threshold. To produce N_2^+ in the ground vibrational level of the $X^2\Sigma_g^+$ ground electronic state of the ion, beginning with the N_2 ground state neutral molecule, requires 15.58 eV. Several excited states and metastable states are energetically accessible even at electron energies $E_e \leq 25$ eV[20,21]. The N_2^+ current increases as the electron energy is raised from threshold to about 40 V. Cross section measurements with N_2^+ as the primary ion show that the observed cross section is independent of the electron energy over the range of 20 - 70 V. This suggests that metastable states of N_2^+ are not interfering with these measurements in the energy range studied in this laboratory.

The vibrational excitation of molecular ions is much more difficult to control than is the electronic excitation. Usually, it is necessary to allow for relaxing collisions between the ions and the parent gas. In both of the ion sources used in this experiment, the parent gas density is too low for a sufficient number of relaxing collisions to occur. Reaction [3] is highly sensitive to the vibrational level of the N_2^+ ion, with the reaction proceeding more than an order of magnitude faster with the N_2^+ in the $v = 1$ level compared with N_2^+ in the $v = 0$ level[22]. Therefore, this reaction provides a check on the degree to which the primary N_2^+ is vibrationally relaxed.

Results from our experiments on reactions [1], [2], and [3] will be described next.

---

[20] Rosenstock, H. M., Draxl, K., Steiner, B. W., and Herron, J. T. (1977) Energetics of Gaseous Ions, *J. Phys. Chem. Ref. Data*, **6**; Suppl. 1.

[21] Lofthus, A., and Krupenie, P. H. (1977) The Spectrum of Molecular Nitrogen, *J. Phys. Chem. Ref. Data*, **6**; 113.

[22] Govers, T. R., Guyon, P. M., Baer, T., Cole, K., Fröhlich, H., and Lavollée, M. (1984) State-Selected Ion-Molecule Reactions: $N_2^+(X, v'')$, $N_2^+(A, v')$ + Ar → N_2 + Ar^+, *Chem. Phys.*, 87;, 373.

4.1. $N_2^+ + D_2 \rightarrow N_2D^+ + D$

We have measured the cross section for Reaction [1] with primary ion energies in the range of 3 to 35 eV (center-of-mass energy range of 0.4 to 4.4 eV). Electron impact on N_2 was used to produce the primary ion beam and C. P. grade D_2 (99.5 percent minimum purity, Scientific Gas Products, Inc.) was used as the target gas. The raw cross section data is shown in Figure 9, plotted

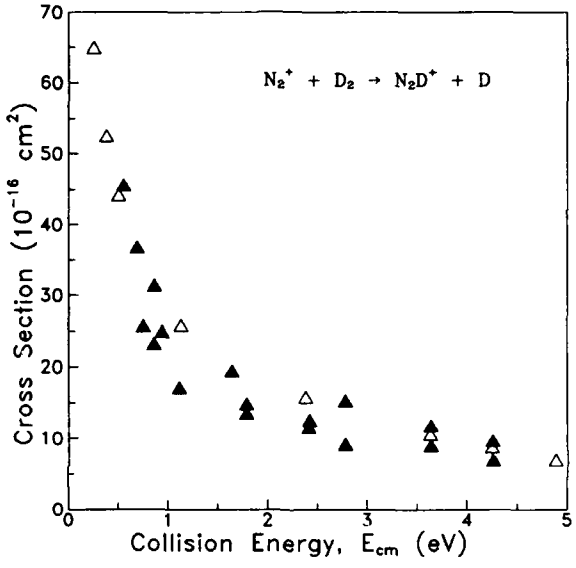

Figure 9: Cross Section Data for Reaction [1] as a Function of the Center-of-Mass Collision Energy. Filled triangles--this work; open triangles--Turner et al.[17]

as a function of the center-of-mass collision energy, along with data from Reference 17 for this reaction in the same energy range. We estimate the uncertainty in our measurements to be ± 20 percent, based on estimates of random errors in the pressure, reaction path length, primary ion beam stability, and ion collection efficiencies. The agreement of our data with Turner et al.[17] is very good, indicating that we are collecting the secondary ions with at least 95 percent efficiency, as expected since the products in this reaction are known to be strongly forward-peaked (laboratory frame)[17].

Our time-of-flight data for the secondary N_2D^+ ions from Reaction [1] are also consistent with the prediction of the spectator stripping mechanism. This mechanism treats this reaction as occurring between the primary ion and a single deuterium atom, rather than the entire D_2 molecule. The N_2^+ is seen as 'stripping' this D atom from its parent (D_2) molecule, while the remainder of the parent molecule (in this case, the second D atom) is a 'spectator' of the reaction and maintains the velocity vector of the target gas. The secondary N_2D^+ ion velocity is therefore equal to the center-of-mass velocity of the N_2^+ + D collision pair. Thus,

$$v_{sec} = v_{prim} (m_{prim} / m_{sec}) \qquad (12)$$

where v_{sec} is the laboratory velocity of the secondary ion, v_{prim} is the laboratory velocity of the primary ion, m_{prim} is the mass of the primary ion, and m_{sec} is the mass of the secondary ion. This transforms to

$$E_{sec} = E_{prim} (m_{prim} / m_{sec}) \qquad (13)$$

where E_{sec} is the laboratory energy of the secondary ion and E_{prim} is the laboratory energy of the primary ion. For Reaction [1], the factor (m_{prim} / m_{sec}) is numerically equal to 0.933. The spectator stripping model therefore predicts that the secondary ions from this reaction are formed with laboratory energies equal to 0.933 times the laboratory energy of the primary ion.

We have measured the laboratory energy for the N_2D^+ secondary ions using the time-of-flight method. In Figure 10, a typical time-of-flight spectrum is shown for the N_2D^+ ions (solid line). The dashed line in Figure 10 shows the time-of-flight spectrum for the primary N_2^+ at the same experimental conditions. Also shown in Figure 10 is the conversion of the time-of-flight to the secondary ion laboratory energy scale. This energy scale is calibrated using the peak position of the primary ion time-of-flight spectrum and the primary ion energy measured in a retardation scan. The laboratory frame energy of the secondary ions is obtained by reading the energy scale shown in Figure 10 at the peak position of the secondary ions.

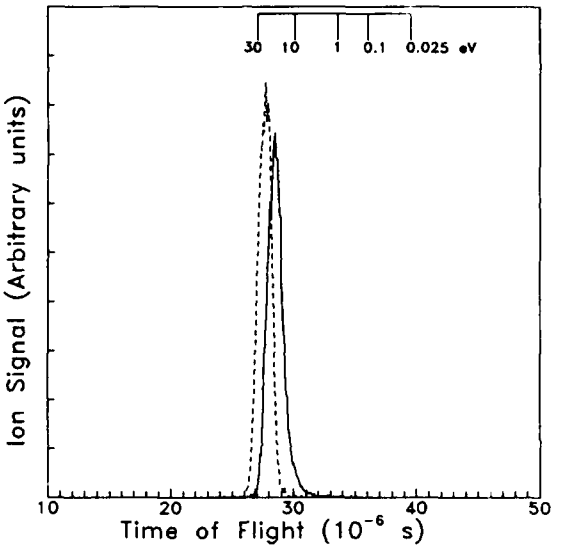

Figure 10: Time-of-Flight Spectra for Primary N_2^+ (20.3 eV) [Dashed] and Secondary N_2D^+ (18.8 eV) [Solid]. The inset scale shows the lab-frame energy corresponding to the secondary ion peak.

The N_2D^+ laboratory energies have been determined with the time-of-flight method over the entire experimental energy range. In Figure 11, these secondary ion laboratory energies are plotted as a function of the laboratory energy of the primary ions, measured using the retardation

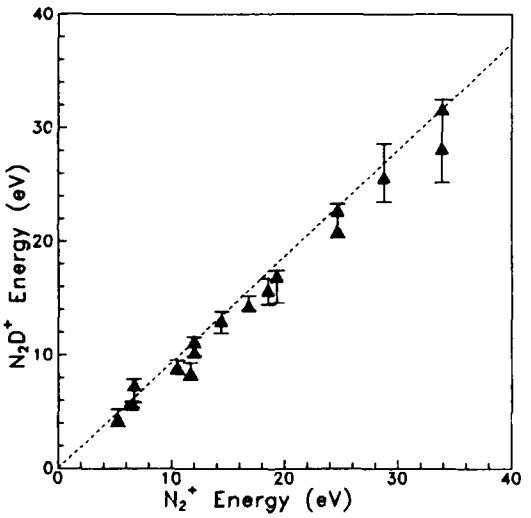

Figure 11: Plot of the Laboratory Energy of the Secondary Ions vs. That of the Primary Ions for Reaction [1]. Dashed line indicates prediction of spectator stripping mechanism.

scan method. The error bars in Figure 11 represent the uncertainty in the calculated energy due to the uncertainty in the peak position in the secondary ion time-of-flight. The larger error bars at higher experimental energies are due to the lower energy resolution at higher ion energies. The dashed line in Figure 11 shows the slope predicted by the spectator stripping mechanism of $y = 0.933\ x$. The excellent agreement between the data and the predicted values indicates that these measurements are reliable under the conditions of strongly forward-peaked product ions.

4.2. $O^+ + H_2O, D_2O \rightarrow O + H_2O^+, D_2O^+$

We have measured Reaction [2] over the center-of-mass energy range from 2 to 15 eV. The primary O^+ is produced by electron impact ionization of CO_2, the H_2O is filtered distilled water (Millipore Milli-Q filtration), and the D_2O is certified 99.8% D (Isotopes™, KOR Inc.). Experimental results for this charge transfer reaction are identical for both isotopes of water.

The results from the time-of-flight measurements for the product ions from Reaction [2] are very different from those for Reaction [1]. A typical D_2O^+ secondary ion time-of-flight measurement is shown in Figure 12. The product ions from Reaction [2] exhibit a near-thermal

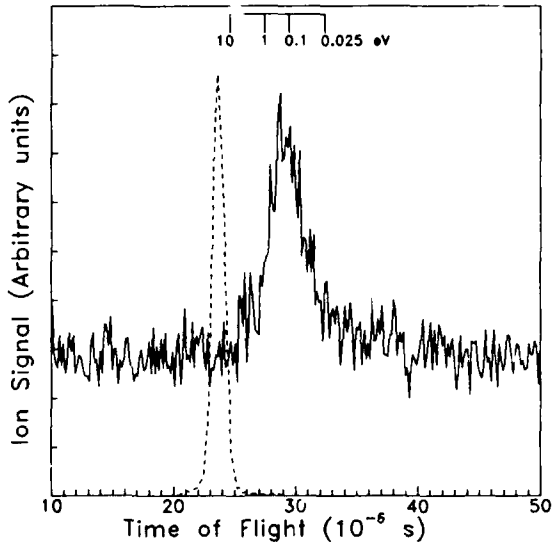

Figure 12: Time-of-Flight Spectra for Primary O^+ (7.7 eV) [Dashed] and Secondary D_2O^+ (0.10 eV) [Solid]. The inset scale shows the lab-frame energy corresponding to the secondary ion peak.

laboratory energy distribution, with the time-of-flight peaks corresponding to about 100 meV throughout the measured energy range.

The raw data from the cross section measurements for Reaction [2] are corrected with Eq. (11) before being displayed in Figure 13. In this figure, the data for the Reaction [2] cross section is plotted as a function of the collision energy in the center-of-mass frame. The corresponding data from Reference 19 is also shown in Figure 13. The excellent agreement between the corrected data from this work and the data of Heninger et al.[19] indicates that the calculated collection efficiency factor provides a good adjustment to our data. The slight

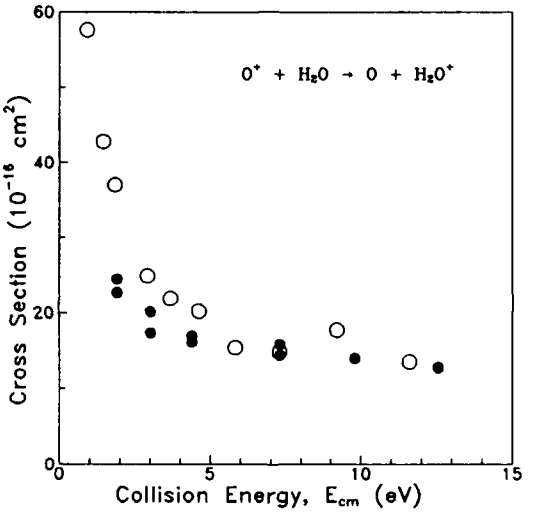

Figure 13: Cross Section Data for Reaction [2]. Closed circles--this work, corrected with Eq. (11); open circles--Heninger et al.[19]

discrepancy in the data at the lowest collision energy may be a consequence of the higher observed product laboratory energy. This higher energy may be due to a broader angular distribution of the products in the center-of-mass frame at that energy, resulting in a lower detection efficiency.

4.3. $N_2^+ + Ar \rightarrow N_2 + Ar^+$

Reaction [3] is strongly dependent on the N_2^+ vibrational distribution. Govers et al.[22] have measured cross sections of Reaction [3] using a vibrationally-selected primary beam. They report

the vibrationally dependent charge transfer cross sections at a center-of-mass energy of 14 eV to be: $v = 0 \Rightarrow \sigma \leq 0.9$ Å^2; $v = 1 \Rightarrow \sigma = 15.6\ (\pm 1.2)$ Å^2; $v = 2 \Rightarrow \sigma = 24.3\ (\pm 2.8)$ Å^2; and $v = 3 \Rightarrow \sigma = 30.3\ (\pm 4.4)$ Å^2. Govers also quotes adjusted data from Kato et al.[23] which gives similar results at a center-of-mass energy of 11.8 eV. Reaction [3] is slightly endothermic (0.16 eV) for $v = 0$, but slightly exothermic (0.1 eV) for $v = 1$.[21]

We have measured Reaction [3] to ascertain the degree of vibrational excitation of N_2^+ produced in our source. Both cross-section and time-of-flight measurements have been performed. The time-of-flight data shows that the Ar^+ produced in this reaction is at near-thermal laboratory translational energy. The reaction cross-section data must therefore be corrected for the system collection efficiency using Eq. (11).

Cross sections were measured as a function of ionizing electron energy using both the EI source and the Colutron source operated in the electron impact mode. The measured cross section is about 13 Å^2 at a center-of-mass energy of about 11.8 eV (see Figure 14). This indicates that N_2^+

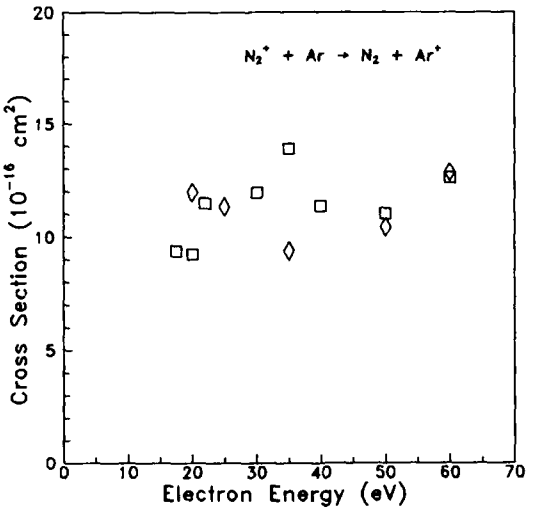

Figure 14: Plot of Cross Section as a Function of Ionizing Electron Energy for Reaction [3] at a Center-of-Mass Collision Energy of 11.8 eV. Squares--EI source; diamonds--Colutron source, electron impact mode. All data has been corrected with Eq. (11) for the system collection efficiency.

---

[23] Kato, T., Tanaka, K., and Koyano, I. (1982) State Selected Ion-molecule Reactions by a TESICO Technique. V. $N_2^+(v)$ + Ar → N_2 + Ar^+, *J. Chem. Phys.*, 77; 834.

vibrational levels higher than the ground state are populated. The cross-section measurements have been nearly independent of the ionizing electron energy over the range of about 17 to 60 eV. Assuming a thermal distribution of the N_2^+ vibrational population, these results are consistent with about 50 to 60 percent of the N_2^+ being in the $v = 1$ or higher vibrational level.

5. FUTURE WORK

Thus far, we have discussed the current design and usage of the double mass spectrometer apparatus. In this section, we outline some recommendations to further improve this experimental apparatus. In its current configuration, the instrument has certain limitations that can be addressed both to improve the accuracy of the measurements and to permit new types of measurements to be made. Currently,

(1) only products scattered in a limited solid angle are collected;

(2) the primary ion beam contains vibrationally excited molecular ions; and

(3) the time-of-flight resolution is low due to the short field-free drift path.

In order to measure an accurate integral cross section, the angular distribution of the ionic reaction products must be known. In the current experiment, this angular distribution is not directly measured, but only inferred from the time-of-flight data in comparisons with known reactions. Alternately, knowledge of the angular distribution is unnecessary *if* one collects all the secondary ions produced in a reaction, regardless of their scattering angle. One technique to greatly increase the product ion collection efficiency is to apply a small electric field in the collision region to extract the product ions from the collision cell. One drawback to that technique is that the primary beam energy resolution is reduced. The "Guided Ion Beam Technique," which Teloy and Gerlich[24] have introduced, achieves a 100 percent secondary ion collection efficiency without simultaneously degrading the primary beam energy resolution. This technique is now used in numerous laboratories in which ion-neutral collisions are studied, and plans are underway to introduce this method into our experiment.

The presence of vibrationally excited molecular ions in the primary ion beam impedes measurements of the type reported here if the ground state cross section is different from that of excited states of the primary ion, for example, the N_2^+ + Ar system treated in Section 4. We also

---

[24] Teloy, E., and Gerlich, D. (1974) Integral Cross Sections for Ion-Molecule Reactions. 1. The Guided Beam Technique, *Chem. Phys.*, **4**; 417.

plan to conduct experiments using optical detection techniques to study chemiluminescence from certain ion-neutral reactions. Analysis of such emissions will yield information both on the electronic excitation of the reaction products and on the vibrational excitation within electronically excited states of the reaction products. For such optical studies to be successful, it is critical to generate an intense primary beam of electronically and vibrationally relaxed ions. To generate such a beam, the excess internal energy of the newly-formed primary ions may be removed by numerous collisions with heavy collision partners, such as the neutral parent gas molecules. Teloy and Gerlich[24] have developed a storage ion source using inhomogeneous rf fields in which ions are trapped for a time, during which they undergo a sufficient number of vibrationally-relaxing collisions. We plan to construct a similar storage ion source to conduct the optical experiments.

Finally, time-of-flight resolution is governed by the initial spatial distribution of the product ions with respect to the time-of-flight axis, the target motion, and the length of the field free path in which they drift. This last factor limits the time-of-flight resolution in the present instrument. We are planning to increase the length of the field-free path to improve the time-of-flight resolution using modifications based on the Guided Ion Beam Technique,[24,25] which uses rf-only fields to store and guide ions. After passing through the Wien filter, the ions will be injected in a first octopole ion guide which conducts the ions through a collision chamber without distorting their forward momentum. The ions produced in ion-molecule reactions will be formed within the octopole; therefore, the collection efficiency of the scattered ions will be independent of the scattering angle. Backward-scattered ions in the laboratory frame can be reflected into the forward direction at the injection end of the ion guide by applying suitable potentials. Upon exiting the collision chamber, the ions will enter a second octopole operating in phase with the first, but floating at a somewhat lower dc potential to accelerate the ions slightly so that near-thermal ions will overcome possible surface potential barriers. The time-of-flight path will primarily consist of the second octopole,

---

[25] Scherbarth, S., and Gerlich, D. (1989) Energy Partitioning in $Ar^+ + O_2$ Collisions at Low Energies: Analysis of Product States by Laser-Induced Predissociation, *J. Chem. Phys.* **90**; 1610.

which will be approximately 15 cm long. This length represents a 30-fold increase in the field-free path, greatly enhancing the time-of-flight resolution. Additionally, the trapping efficiency of the octopole depends on the perpendicular velocity component of the ions and the rf amplitude, so variation of the rf amplitude can yield information on the angular distribution of the scattered ions, as shown by Scherbarth and Gerlich.[25] This information may be sufficient to distinguish between large angle scattering and internal excitation of secondary ions.

6. CONCLUSION

In this technical report we have reported the techniques used presently in the Space Physics Division to study ion-neutral collisions at suprathermal energies. The combined measurement of reaction cross sections and product kinetic energy release offers good insight into the various possible processes. The apparatus described herein is being used to measure the reactions of the primary ions N_2^+, O^+, and N^+ with the target gases H_2O and CO_2; and has also been used to measure the reaction between primary H_2O^+ and target gas H_2O in isotopic labelling experiments. Several publications are in progress as a result of this work, including:

1) "Cross Section and Product Time-of-Flight Measurements of the Reaction of N_2^+ with H_2O and D_2O at Suprathermal Energies" by R. A. Dressler, J. A. Gardner, R. H. Salter, F. J. Wodarczyk, and E. Murad, *J. Chem. Phys.*, in press;

2) "Cross Sections and Product Kinetic Energy Analysis of H_2O^+-H_2O Collisions at Suprathermal Energies" by C. R. Lishawa, R. A. Dressler, J. A. Gardner, R. H. Salter, and E. Murad, in preparation; and

3) "Cross Section and Product Time-of-Flight Measurements of the Reaction of N_2^+ and N^+ with CO_2 at Suprathermal Energies" by J. A. Gardner, R. A. Dressler, R. H. Salter, and E. Murad, in preparation.

7. REFERENCES

1. Narcisi, R. S., Trzcinski, E., Federico, G., Wlodyka, L., and Delorey, D., (1983) *The Gaseous and Plasma Environment Around the Space Shuttle*, AIAA-83-2659, 183.

2. Grebowsky, J. M., Pharo, M. W., Taylor, H. A., and Eberstein, I. J., (1987) Thermal Ion Perturbations Observed in the Vicinity of the Space Shuttle, *Planet. Space Sci.*, **35**; 501.

3. Hastings, D. E., Gatsonis, N. A., and Mogstad, T. (1988) A Simple Model for the Initial Phase of a Water Plasma Cloud About a Large Structure in Space, *J. Geophys. Res.*, **93**; 1961.

4. Caledonia, G. E., Person, J. C., and Hastings, D. E. (1987) The Interpretation of Space Shuttle Measurements of Ionic Species, *J. Geophys. Res.*, **92**; 273.

5. Hunton, D. E., and Calo, J. M. (1985) Low Energy Ions in the Shuttle Environment: Evidence for Strong Ambient-Contaminant Interactions, *Planet. Space Sci.*, **33**; 945.

6. Murad, E. (1985) Implications of Mass Spectrometric Measurements on Space Shuttle, *Planet. Space Sci.*, **33**; 421.

7. Jursa, A., ed. (1985) *Handbook of Geophysics and the Space Environment*, ADA 167000.

8. Elgin, J. B., Cooke, D. C., Tautz, M., and Murad, E., Modeling of Atmospherically-Induced Gas Phase Optical Contamination from Orbiting Spacecraft, *J. Geophys. Res.*, submitted for publication.

9. Maier, W. B., and Murad, E. (1971) Study of Collisions between Low-Energy N^+ and N_2: Reaction Cross Sections, Isotopic Compositions, and Kinetic Energies of the Products, *J. Chem. Phys.*, **55**; 2307.

10. Udseth, H., Giese, C. F., and Gentry, W. R. (1973) Transition Probabilities and Differential Cross Sections for Vibrational Excitation in Collisions of H^+ with H_2, HD, and D_2, *Phys. Rev. A*, **8**; 2483.

11. Wahlin, L. (1964) The Colutron, a Zero Deflection Isotope Separator, *Nuclear Instruments and Methods*, **27**; 55.

12. Dahl, D. A., Delmore, J. E., and Appelhaus, A. D. (1990) SIMION PC/PS2 electrostatic lens design program, *Rev. Sci. Instrum.*, **61**; 607.

13. See for example: Paul, W., and Steinwedel, H. (1953) Ein neues Massenspektrometer ohne Magnetfeld, *Z. Naturforsch*, **8a**; 448; Paul, W., and Raether, M. (1955) Das elektrische Massenfilter", *Z. Physik*, **140**; 262; Paul, W., Reinhard, H. P., and von Zahn, U. (1958) Das elektrische Massenfilter als Massenspektrometer und Isotopentrenner, *Z. Physik*, **152**; 143.

14. Burrous, C. N., Lieber, A. J., and Zaviantseff, V. T. (1967) Detection Efficiency of a Continuous Channel Electron Multiplier for Positive Ions, *Rev. Sci. Instr.*, **38**; 1477.

15. Potter, W. E., and Mauersberger, K. (1972) Spiral Electron Multiplier Operation Characteristics Using Positive Ions, *Rev. Sci. Instr.*, **43**; 1327.

16. Dressler, R., Gremaud, M., Chassot, P.-H., and Allan, M. (1985) The Control of a Negative Ion Mass Spectrometer by an Apple II Computer: A Versatile Interface Card for Control of Chemical Instrumentation, *Chimia*, **39**; 327.

17. Turner, B. R., Fineman, M. A., and Stebbings, R. F. (1965) Crossed-Beam Investigation of N_2D^+ Production in N_2^+-D_2 Collisions, *J. Chem. Phys.*, **42**; 4088.

18. Paulson, J. F., Dale, F., and Studniarz, S. A. (1970) Study of Ion-Neutral Reactions with a Time-of-Flight Double Mass Spectrometer, *Intl. J. Mass Spec. and Ion Phys.*, **5**; 113.

19. Heninger, M., Fenistein, S., Mauclaire, G., Marx, R., and Murad, E. (1989) Review of the Reaction of O^+ with H_2O and Its Bearing on Composition Measurements from the Space Shuttle, *Geophys. Res. Lett.*, **16**; 139.

20. Rosenstock, H. M., Draxl, K., Steiner, B. W., and Herron, J. T. (1977) Energetics of Gaseous Ions, *J. Phys. Chem. Ref. Data*, **6**; Suppl. 1.

21. Lofthus, A., and Krupenie, P. H. (1977) The Spectrum of Molecular Nitrogen, *J. Phys. Chem. Ref. Data*, **6**; 113.

22. Govers, T. R., Guyon, P. M., Baer, T., Cole, K., Fröhlich, H., and Lavollée, M. (1984) State-Selected Ion-Molecule Reactions: $N_2^+(X, v'')$, $N_2^+(A, v')$ + Ar → N_2 + Ar^+, *Chem. Phys.*, 87;, 373.

23. Kato, T., Tanaka, K., and Koyano, I. (1982) State Selected Ion-molecule Reactions by a TESICO Technique. V. $N_2^+(v)$ + Ar → N_2 + Ar^+, *J. Chem. Phys.*, **77**; 834.

24. Teloy, E., and Gerlich, D. (1974) Integral Cross Sections for Ion-Molecule Reactions. 1. The Guided Beam Technique, *Chem. Phys.*, **4**; 417.

25. Scherbarth, S., and Gerlich, D. (1989) Energy Partitioning in Ar^+ + O_2 Collisions at Low Energies: Analysis of Product States by Laser-Induced Predissociation, *J. Chem. Phys.* **90**; 1610.